A Constrained Kalman Filter for Rigid Body Systems with Frictional Contact

Patrick Varin and Scott Kuindersma

Harvard University, Cambridge MA 02138, USA,
`varin@g.harvard.edu`, `scottk@seas.harvard.edu`

Abstract. Contact interactions are central to robot manipulation and locomotion behaviors. State estimation techniques that explicitly capture the dynamics of contact offer the potential to reduce estimation errors from unplanned contact events and improve closed-loop control performance. This is particularly true in highly dynamic situations where common simplifications like no-slip or quasi-static sliding are violated. Incorporating contact constraints requires care to address the numerical challenges associated with discontinuous dynamics, which make straightforward application of derivative-based techniques such as the Extended Kalman Filter impossible. In this paper, we derive an approximate maximum a posteriori estimator that can handle rigid body contact by explicitly imposing contact constraints in the observation update. We compare the performance of this estimator to an existing state-of-the-art Unscented Kalman Filter designed for estimation through contact and demonstrate the scalability of the approach by estimating the state of a 20-DOF bipedal robot in realtime.

Keywords: State Estimation, Dynamics, Kalman Filter, Rigid Body Contact, Optimization

1 Introduction

Achieving reliable state estimation in the presence of uncertain dynamics and noisy measurements is a prerequisite for developing robust feedback controllers. This is particularly true for robots that experience impacts or transitions between static and sliding contact. When these discontinuous events are not explicitly accounted for, they can lead to large estimation errors and catastrophic failures—highlighting the need for efficient and practical estimation algorithms that reason about whole-body contact interactions.

Although state estimation for systems with differentiable dynamics has been studied extensively, the problem changes dramatically when robots interact with their environment through rigid body contact. For example, a rigid object colliding with, then sliding across a flat surface is subject to non-linear manifold constraints, discontinuous changes in velocity, and Coulomb friction. This requires machinery beyond standard recursive estimation approaches such as the Extended Kalman Filter (EKF) [1].

In this paper, we develop an approximate maximum a posteriori (MAP) estimator using ideas from the constrained Kalman filter [2] and the complementarity constraints proposed originally by Stewart and Trinkle [3]. Our approach simultaneously estimates the system state as well as the contact forces during each update, and guarantees that they are physically consistent with our time-stepping model of rigid body contact.

We compare this formulation directly to a state-of-the-art Unscented Kalman Filter (UKF) [4] using a simulated example where the UKF fails to describe the qualitative behavior of a single rigid body system. We also evaluate the proposed filter on a publicly accessible physical planar pushing dataset and compare estimation performance against motion capture measurements using the Cassie bipedal robot walking overground.

2 Related Work

Traditional approaches to estimation in the presence of rigid body contact, such as locomotion, often use simplified dynamic models to perform estimation updates. Successful approaches for estimation on walking robots have used models such as the linear inverted pendulum to perform estimation on the floating base alone [5–7], while others factor the body dynamics into the floating base and the joint angles, estimating them separately, and use information from the foot kinematics to help localize the floating base [8–12]. These approaches sacrifice accuracy by ignoring the dynamic interactions between the joints and the floating base, but more importantly they often rely on simplifying assumptions like no slip at the contact points and the presence of accurate contact sensors to resolve the active contact mode. As a result, the robot is restricted to conservative behaviors that avoid slipping; violating this assumption quickly causes the filter to fail.

Another approach is to use a hybrid model to perform state estimation [13], unfortunately the reliance on accurate contact sensors makes the filter sensitive to unmeasured contacts that can cause large estimation errors. Other work has been done to estimate external forces applied to articulated rigid body systems, so contact forces can be inferred without direct measurement from a contact sensor [14]. This is a big step towards full body estimation through contact by reasoning about external forces applied at arbitrary locations, but doesn't address the dynamics of contact that are responsible for producing these forces.

Several estimation techniques have been explored that attempt to explicitly model contact dynamics. For estimation in low dimensional state spaces, Koval et al. developed the Contact Particle Filter (CPF)[15] and the Manifold Particle Filter (MPF) [16]. The main insight behind the CPF and the MPF was that contact constrains the dynamics evolve on a lower dimensional manifold of state space (i.e. the *contact manifold*). This problem is inherent to sampling-based approaches because the probability of sampling a lower dimensional manifold is zero, resulting in particle starvation. The CPF gets around this by sampling from a mixture model over all of the contact manifolds. The MPF takes advantage of this low dimensional contact manifold to focus sampling efforts, allowing the particle filter to extend to higher dimensions. Unfortunately, the curse of di-
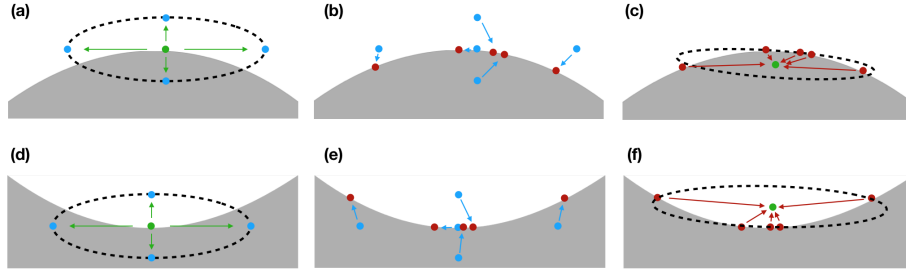
Fig. 1: Two illustrations of fundamental problems associated with the UKF in the presence of the inequalities associated with contact. When sample points are generated (a and d) samples are either infeasible or have different contact modes than the mean estimate. In the first sequence (a-c) the resulting estimate (c) is infeasible even though all of the samples are feasible. In the second sequence (d-f) the resulting estimate (f) is feasible, but has a contact mode that is different from any of the individual sample points. In our experience this is the more common behavior, biasing the estimate away from the contact manifold.

mensionality makes the particle filter intractable as the state dimension grows, because the number of necessary particles grows exponentially with the state dimension.

To allow the estimation problem to scale to higher dimensions Lowrey et al. [4] developed a UKF to perform estimation through contact. The UKF avoids the curse of dimensionality by approximating the state distribution as Gaussian, which affords an efficient representative sample set that grows linearly, rather than exponentially with the state dimension. In our experience the UKF fails to accurately describe contact dynamics for the same reasons that cause particle starvation in the particle filter; it is inaccurate to draw sample points from a full Gaussian distribution when the dynamics are evolving on a lower dimensional contact manifold. This causes the UKF to sample infeasible states that can produce non-physical behavior. Figure 1 illustrates two situations that cause the UKF to produce poor estimates in the presence of contact. In practice, the most common behavior is that the UKF produces estimates that are biased away from the contact manifold.

There have been a few examples of derivative-based approaches to estimation through contact. Earlier work by Lowrey et al. developed an EKF using a smooth approximation to the contact dynamics [17]. This filter was prone to divergence during contact events because of the large derivatives involved when approximating the discontinuous dynamics with a smooth model. A more robust approach to derivative-based estimation is based on constrained optimization [2], which does not sacrifice the integrity of the model by making a smooth approximation to the dynamics. Xinjilefu developed a variation of a constrained dynamic estimator for bipedal walking [10]. Xinjilefu's approach uses contact sensors on the feet to infer the contact mode, and solves for the estimated state and contact forces with a quadratic program by assuming that the feet cannot slip. These assumptions limit the use of this filter to conservative walking on robots with

contact sensors on the feet, and is not easily extensible to different domains, e.g. manipulation, where sliding contact is more prevalent.

3   Background

The filter we present here is most reminiscent of the constrained optimization work by Xinjilefu [10], but provides a more general framework for estimation through contact and can be applied to arbitrary rigid body systems. In order to develop the Contact Constrained Kalman Filter (CCKF), we first describe our model of rigid body contact and the constraints imposed by this model, then we incorporate these constraints into the constrained Kalman filtering framework.

3.1   Contact Constraints

Stewart and Trinkle [3] developed a time-stepping rigid body model for contact as a constraint satisfaction problem. These dynamics compute the state at the next timestep as the solution to a linear complementarity problem (LCP). This problem can be solved with a variety of techniques such as, Dantzig's algorithm [18], Lemke's algorithm [19], PATH [20], etc. Anitescu and Potra [21] later proved that this LCP is solvable. These timestepping dynamics form the basis for many popular physics engines including Bullet [22], Open Dynamics Engine [23], and Dynamic Animation and Robotics Toolkit [24]. We reintroduce these constraints and develop their physical intuition here.

We can approximate the continuous dynamics of a rigid body system with a discrete time system using a semi-implicit Euler update,

$$v_{k+1} = v_k + \Delta t H_k^{-1} \left(B_k u_k - C_k - G_k + J_k^T \lambda_k \right) \tag{1}$$

$$q_{k+1} = q_k + \Delta t v_{k+1}, \tag{2}$$

where q_k and v_k are the generalized position and velocity of the system, H, C, and G represent the mass matrix, Coriolis terms, and gravitational forces, respectively, B maps control inputs to generalized forces, and J is the Jacobian that maps external forces, λ, to generalized forces. In the absence of contact, $\lambda = 0$, so Equations (1) and (2) are sufficient to compute the dynamics. During contact, however, we compute λ by considering contact constraints.

The first constraints relate to collisions and the normal force required to prevent interpenetration. Both the signed distance between two bodies, $\phi(q)$, and the normal force, λ^n, must be non-negative. Furthermore, the contact forces can only be nonzero when two bodies are in contact. These constraints can be written as

$$\phi(q) \geq 0, \qquad \lambda^n \geq 0, \qquad \phi(q)^T \lambda^n = 0. \tag{3}$$

This last constraint says that if the bodies are touching, $\phi = 0$, the force is allowed to be non-negative, $\lambda^n \geq 0$, but if the bodies are not touching, $\phi > 0$, then there can be no contact force between them, $\lambda^n = 0$. This is known as a complementarity constraint and can be written succinctly as

$$\phi(q) \geq 0 \perp \lambda^n \geq 0. \tag{4}$$

Because ϕ is generally a nonlinear function of q, this is a *nonlinear* complementarity constraint. For computational reasons we will instead use the *linear* complementarity constraint

$$\phi_k + \nabla\phi(q_{k+1} - q_k) \geq 0 \perp \lambda_k^n \geq 0. \tag{5}$$

In addition to non-penetration, we also want to satisfy constraints on tangential friction. Rather than using the usual second order Coulomb friction cone, we use a polyhedral approximation to the friction cone, allowing us to remain within the LCP framework. We construct the contact force, λ, by decomposing it into the normal and tangential components,

$$\lambda = n\lambda^n + D\beta, \;\; \beta \geq 0, \tag{6}$$

where $n \in \mathbb{R}^{3\times 1}$ is the surface normal, and the columns of $D \in \mathbb{R}^{3\times d}$ are unit vectors that positively span the tangent plane. In practice we use $d = 4$, but any $d \geq 3$ would work where larger values provide a more accurate approximation of the friction cone at the expense of additional decision variables. We can then write the polyhedral friction cone constraint as

$$\mu\lambda^n - e^T\beta \geq 0. \tag{7}$$

It is assumed that the tangential friction respects the maximum dissipation principle (i.e. that contact forces are chosen to maximize dissipation of kinetic energy) so the tangential contact force must be an optimal point for the optimization problem

$$\lambda^t = \;\; \underset{\lambda^t}{\arg\min} \;\; v^T J^T \lambda \tag{8}$$

$$\text{subject to } \mu\lambda^n - e^T\beta \geq 0 \tag{9}$$

$$\beta \geq 0. \tag{10}$$

The first-order necessary conditions, i.e. Karush-Kuhn-Tucker (KKT) conditions, for this problem can be written as

$$D^T J v + \eta^T e \geq 0 \perp \beta \geq 0, \tag{11}$$

$$\mu\lambda^n - e^T\beta \geq 0 \perp \eta \geq 0, \tag{12}$$

where η is a Lagrange multiplier that can be interpreted as the magnitude of the tangential velocity. Intuitively the first condition enforces that the force of friction opposes the tangential velocity, while the second condition ensures that there can only be tangential velocity (sliding) when force of friction is on the edge of the friction cone. Together Equations (1-2), (5), and (11-12) specify Stewart and Trinkle's time stepping rigid body dynamics, and will be the foundation of the filter we develop here.
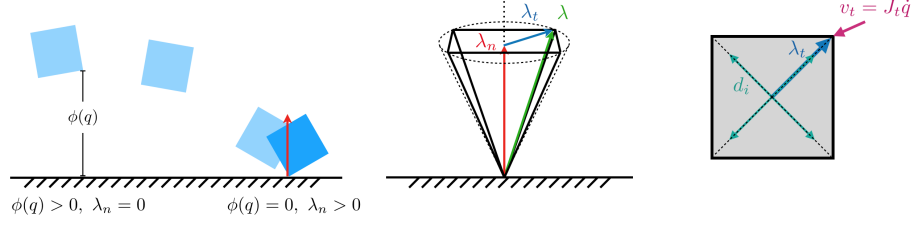
Fig. 2: Contact constraints that govern rigid body contact dynamics. Left: Non-penetration and positive normal force, the normal force can only non-zero if the signed distance function, ϕ, is zero. Center: Polyhedral friction cone, we can approximate the Coulomb friction cone with a polyhedral cone. Right: Complementarity between tangential velocity and tangential friction. There can only be tangential velocity when the force of friction is on the edge of the friction cone.

3.2 Constrained Kalman Filter

We can build these contact constraints into a MAP estimator using the constrained Kalman Filter [2]. Consider the discrete time stochastic system:

$$x_{k+1} = f(x_k, u_k) + w_k \qquad\qquad w_k \sim \mathcal{N}(0, Q) \qquad (13)$$

$$y_k = h(x_k) + v_k \qquad\qquad v_k \sim \mathcal{N}(0, R), \qquad (14)$$

where x is the state, u is a control input, and y is a noisy measurement. If the prior on x is Gaussian with mean x_{k-1} and covariance P_{k-1}, then we can compute the mean and covariance of an approximate posterior by linearizing the dynamics, $F = \frac{\partial f}{\partial x}$, and the observation function, $H = \frac{\partial h}{\partial x}$, and using the Extended Kalman Filter (EKF) updates:

$$x_k^- = f(x_{k-1}, u_{k-1}) \qquad (15)$$

$$P_k^- = FP_{k-1}F^T + Q \qquad (16)$$

$$x_k = x_k^- + K(y_k - h(x_k^-)) \qquad (17)$$

$$P_k = (I - KH_k)P_k^-, \qquad (18)$$

where K is the Kalman gain.

Because the mean of the Gaussian distribution is also the mode, the observation update (17) can be interpreted as an approximate maximum a posteriori (MAP) estimate—up to the linearization of $f(\cdot)$ and $h(\cdot)$—that can be computed in closed form because the negative logarithm of a Gaussian pdf is a convex quadratic function.

This interpretation of the Kalman filter as the MAP estimator allows us to naturally incorporate dynamic constraints into the filter by writing the observation update as a constrained optimization problem:

$$\underset{x}{\text{minimize}} \qquad \Delta x^T P^{-1} \Delta x + (\tilde{y} - H\Delta x)R^{-1}(\tilde{y} - H\Delta x) \qquad (19)$$

$$\text{subject to} \qquad g_{\text{eq}}(x) = 0 \qquad (20)$$

$$g_{\text{in}}(x) \le 0. \qquad (21)$$

where $\Delta x = x_k - x_k^-$ is the state correction and $\tilde{y}_k = y_k - h(x_k^-)$ is the innovation. If the constraints $g_{eq}(\cdot)$ and $g_{in}(\cdot)$ are linear then this can be solved efficiently as a quadratic program (QP). This was the approach used by Xinjilefu [10] in developing the estimator for the Atlas humanoid robot. The technique that we will develop here is similar in spirit, but does not rely on contact sensors to resolve the active contacts, and allows for dynamic contact interactions such as slipping by taking a fundamentally different approach to contact.

4 Contact Constrained Kalman Filter

The contact constraints developed in Section 3.1 suggest that in order to perform state estimation through contact we need to consider both the state, x, as well as the contact forces, λ. While the Stewart-Trinkle dynamics compute the contact forces as an implicit function of the state, this mapping is discontinuous and cannot be linearized, precluding its use in the EKF framework. To develop the Contact Constrained Kalman Filter (CCKF) we apply the constrained Kalman filtering approach and explicitly optimize over both the state and the contact forces.

We can rewrite the discrete time dynamics (Equations 1 and 2) as

$$x_k = \hat{x}_k + \hat{J}_{k-1}^T \lambda_k, \qquad\qquad \hat{J}^T = \begin{bmatrix} \Delta t^2 H^{-1} J^T \\ \Delta t H^{-1} J^T \end{bmatrix}, \qquad (22)$$

where $\hat{x}_k$ is the state of the unconstrained system at time k (capturing the state changes from the inputs, gravity, etc.) and $\hat{J}^T$ maps contact forces to changes in the generalized coordinates. The objective for the optimization function then becomes

$$\left(\begin{bmatrix} x_k \\ \lambda_k \end{bmatrix} - \begin{bmatrix} \hat{x}_k \\ 0 \end{bmatrix} \right)^T \left[I, -\hat{J}_{k-1} \right]^T \left(P_k^- \right)^{-1} \left[I, -\hat{J}_{k-1} \right] \left(\begin{bmatrix} x_k \\ \lambda_k \end{bmatrix} - \begin{bmatrix} \hat{x}_k \\ 0 \end{bmatrix} \right)$$
$$+ (\tilde{y}_k - H_x \Delta x - H_\lambda \lambda)^T R^{-1} (\tilde{y}_k - H_x \Delta x - H_\lambda \lambda), \quad (23)$$

and the contact constraints become

$$\begin{bmatrix} nJ & 0 & 0 \\ 0 & DJ & E \\ 0 & 0 & I \end{bmatrix} \begin{bmatrix} q_k \\ v_k \\ \eta_k \end{bmatrix} + \begin{bmatrix} \phi - nJq_{k-1} \\ 0 \\ 0 \end{bmatrix} \geq 0 \perp \begin{bmatrix} I & 0 \\ 0 & I \\ \tilde{\mu} & -E^T \end{bmatrix} \begin{bmatrix} \lambda_k^n \\ \beta_k \end{bmatrix} \geq 0. \qquad (24)$$

Note that the complementarity constraints separate the decision variables nicely into two sets that together form a bilinear constraint. These can be loosely interpreted as the primal variables, x, η, and the dual variables λ^n, β associated with contact dynamics. Defining these new variables as $\tilde{x} = \begin{bmatrix} x^T & \eta^T \end{bmatrix}^T$ and $\tilde{z} = \begin{bmatrix} \lambda^{nT} & \beta^T \end{bmatrix}^T$ we can write down the full optimization problem for the observation update concisely as

$$\operatorname*{minimize}_{x,z} \quad \begin{bmatrix} \tilde{x} \\ \tilde{z} \end{bmatrix}^T Q \begin{bmatrix} \tilde{x} \\ \tilde{z} \end{bmatrix} - l^T \begin{bmatrix} \tilde{x} \\ \tilde{z} \end{bmatrix}^T \qquad (25)$$

$$\text{subject to} \quad A\tilde{x} + b \geq 0 \perp C\tilde{z} \geq 0. \qquad (26)$$

Algorithm 1: The Contact Constrained Kalman Filter

---

1 initialize x and P;
2 $f(x)$ is the unconstrained dynamics from (1) and (2) with $\lambda = 0$;
3 $h(x, \lambda)$ is the observation function;
4 while *true* **do**
| /* compute the process update with no contact forces   */
5 | $\hat{x} = f(x)$;
6 | $F = \frac{\partial f}{\partial x}$;
7 | $P^- = FPF^T$;
| /* compute the observation update via constrained minimization */
8 | $\tilde{y} = y - h(\hat{x})$;
9 | $H_x = \frac{\partial h}{\partial x}$ and $H_\lambda = \frac{\partial h}{\partial \lambda}$;
10 | $x, \lambda = \arg\min$ (23) subject to (24);
11 | $P = P^- - P^- H_x^T (H_x P^- H_x^T + R)^{-1} H_x P^-$;
12 end

As we noted, this optimization problem doesn't require contact sensors to resolve the contact mode, but information from contact sensors can be naturally incorporated via the contact force dependence in the observation function $h(x, \lambda)$.

4.1   Quadratic Program with Complementarity Constraints

In order to implement the CCKF we must solve the optimization problem defined by (23) and (24). This problem is a special case of a quadratic program with complementarity constraints (QPCC). In our experiments, we chose to solve this problem via mixed-integer optimization. We can formulate the complementarity constraint by introducing a binary variable, y, that determines which of the equality constraints are active. This results in the mixed integer quadratic program (MIQP):

$$\underset{x,y,z}{\text{minimize}} \begin{bmatrix} x \\ z \end{bmatrix}^T Q \begin{bmatrix} x \\ z \end{bmatrix} - l^T \begin{bmatrix} x \\ z \end{bmatrix}^T \tag{27}$$

$$\text{subject to } Ax + b \geq 0 \tag{28}$$

$$Cy \geq 0 \tag{29}$$

$$y^T(Ax + b) = 0 \tag{30}$$

$$(1 - y)^T Cz = 0 \tag{31}$$

$$y \in \{0, 1\}^N. \tag{32}$$

We solve this MIQP using the commercial optimization package Gurobi [25] that employs a branch-and-bound method to find the exact solution. Warm starting the binary variable at each time step allows the optimizer to quickly prune the branch-and-bound tree. As we show in our results, this has a positive impact on both the mean and variance of update times.

5   Results

We evaluate the Contact Constrained Kalman Filter in three scenarios.

1. We demonstrate the practical shortcomings of the state-of-the-art UKF in a simple single 6-DOF rigid body scenario where the UKF fails to describe the system's behavior, but the CCKF succeeds.
2. We validate the performance of the CCKF during sliding using examples from a large physical planar pushing dataset.
3. We demonstrate that the filter scales to more complex systems by evaluating estimation and timing performance on a 20-DoF physical biped.

The filter parameters for each of these experiments are detailed in Table 1. Because the UKF doesn't successfully capture the behavior of the simple toy example in the first experiment, we do not use the UKF as a baseline in subsequent experiments. For example, in the planar pushing experiment the UKF predicts states that are non-planar, hovering above the pushing surface, whereas the CCKF correctly predicts planar states.

5.1   Simulated Data

One predicted advantage of the CCKF over the comparable state-of-the-art UKF approach [4] is that the UKF tends to produce non-physical behavior near the contact manifold (Figure 1) while the CCKF handles inequalities arising from the contact manifold by optimizing over a truncated Gaussian. To compare the performance of the proposed filter and the UKF on a simple system, we evaluated both filters on simulated data of a rectangular prism rotating and falling onto flat ground. We approximated the sensor data that would be obtained from system with an IMU and visual or proprioceptive sensors by generating noisy position, gyroscope, and accelerometer measurements. Since both approaches use a different formulation of rigid body dynamics, we chose a simulator that uses neither. Forward simulation was performed using a compliant contact model in Drake [26] that approximates rigid body contact but allows for slight interpenetration according to a user specified Young's Modulus. In our experiments we used all of the default parameters except for the friction coefficients for which we used $\mu = 1.0$ to be consistent with our implementation of the UKF. Both filters used the same parameters, operating at 100Hz. The covariance parameters R and P_0 were chosen to reflect the true measurement noise and initial state error, while Q was chosen so that both filters converged to steady state before the first contact event.

Figure 3 illustrates the performance of both filters from 20 randomly initialized state estimates for a single forward simulation. The UKF performs well up until the second collision, at which point the contact manifold constrains two degrees of freedom, corresponding to at least two infeasible sigma points, and the filter begins to diverge. After the brick has settled, we can see that the state estimate is biased above the ground, away from the contact manifold. The CCKF, however, shows good tracking performance throughout the entire trajectory.

5.2   Planar Pushing Dataset

In order to demonstrate the performance of the filter during frictional sliding, we evaluated the filter on the PUSH dataset, a planar pushing dataset collected by the MCube lab at MIT [27]. This dataset contains pose data of various shapes
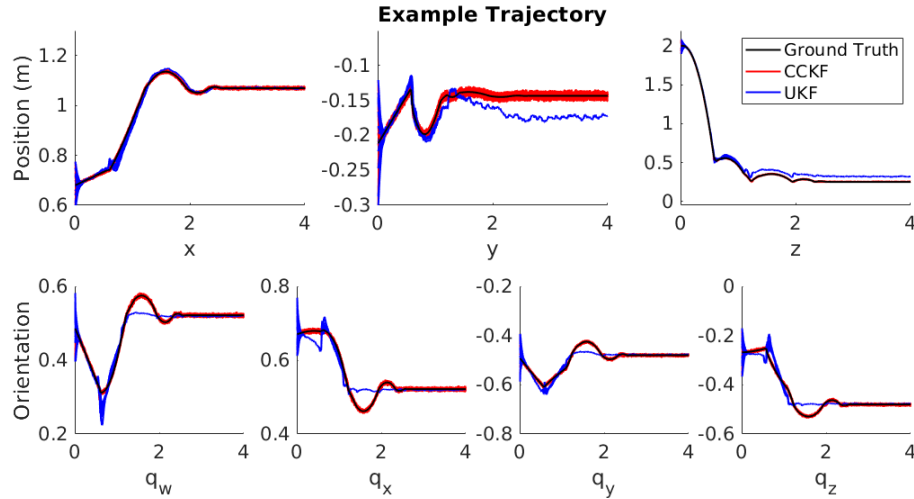
Fig. 3: Simulation results of a brick falling on flat ground. Top: the CCKF accurately estimates the brick trajectory through the contacts, while the UKF struggles near the contact manifold.

being pushed on a number of surfaces. While many of the pushing examples from this dataset involve only quasi-static motion, which does not highlight the full capability of this filter, there are a number of examples of aggressive pushing where the object continues to slide after contact with the manipulator is broken.

We selected the most aggressive (largest acceleration) pushes of the rect1 object, a rectangular object, on delrin, which was reported to have the most consistent coefficient of friction of the surfaces used in the dataset (0.14 ± 0.016). Detailed geometric and inertial parameters for this object are provided with the dataset. The coefficient of friction was set to the experimentally reported mean.

We ran the filter on pose data that was corrupted with zero mean Gaussian noise. The filter parameters were empirically chosen to maximize the filter performance, except for R which was chosen to reflect the true added measurement noise. Figure 4 illustrates the filter performance on an example sliding trajectory. When the coefficient of friction is set correctly the filter exhibits good performance, correctly estimating the time at which the object comes to rest. When the friction coefficient is too large the velocity estimate to drops to zero prematurely, and when the friction is too small the estimate overshoots the true state. The observation update is able to correct the position and orientation for all examples with zero steady state error, except in the frictionless example where the dynamics are sufficiently different.

It is interesting to note that while the observation update is able to correct errors in the position, it cannot correct the velocity estimate because it is not directly observed. Figure 4, illustrates that a misspecified model, such as incorrect friction, can produce velocity trajectories that are inconsistent with the position trajectories. Such inconsistencies may be improved with a richer measurement model that is able to correct the inconsistent velocities in the observation update,
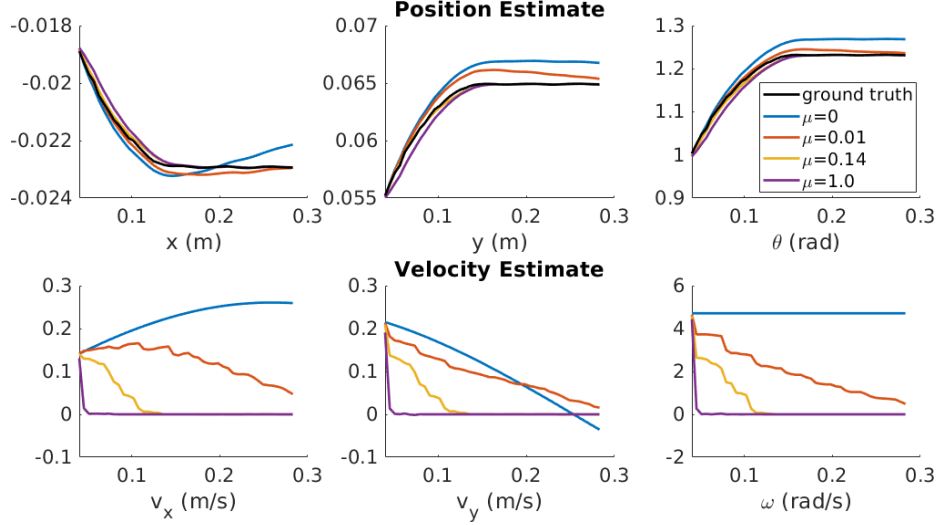
Fig. 4: The mean state estimates from an example sliding trajectory with various coefficients of friction. $\mu = 0.14$ has the best agreement and was the mean coefficient of friction reported with the experimental data.

or a longer filter horizon that can use multiple sequential position measurements to inform the velocity estimate.

5.3   State Estimation for a Biped

To demonstrate that this filter scales to complex robots, we collected data using a Cassie bipedal robot walking in two scenarios: a scenario that is indicative of stable walking on flat ground and a scenario where we lubricated the walking surface, causing the robot to slip.

Cassie has 20 degrees of freedom (DOF): 6 DOF arise from the floating base, 10 DOF in the joints are directly actuated, and the 4 remaining DOF are stabilized with stiff springs. Additionally, each leg contains a kinematic loop that are represented as additional constraints in the filter. We used the inertial parameters and the spring constants provided by the manufacturer. Cassie is outfitted with a 6-axis IMU and 14 joint encoders that measure the position and velocity of the joints. The prepackaged software provides an orientation estimate from the IMU, but does not log the accelerometer data, so we used the orientation estimate as a sensor in our experiments in lieu of the underlying accelerometer data.

Walking The walking experiment was conducted in a motion capture studio to gather ground truth position data. The robot walked around the motion capture studio for approximately 5 minutes, then onboard sensor data was synchronized in time with the motion capture measurements.

Figure 5 illustrates the performance of the estimator during a typical step and over a large step sequence. Starting from a 20 random initial conditions
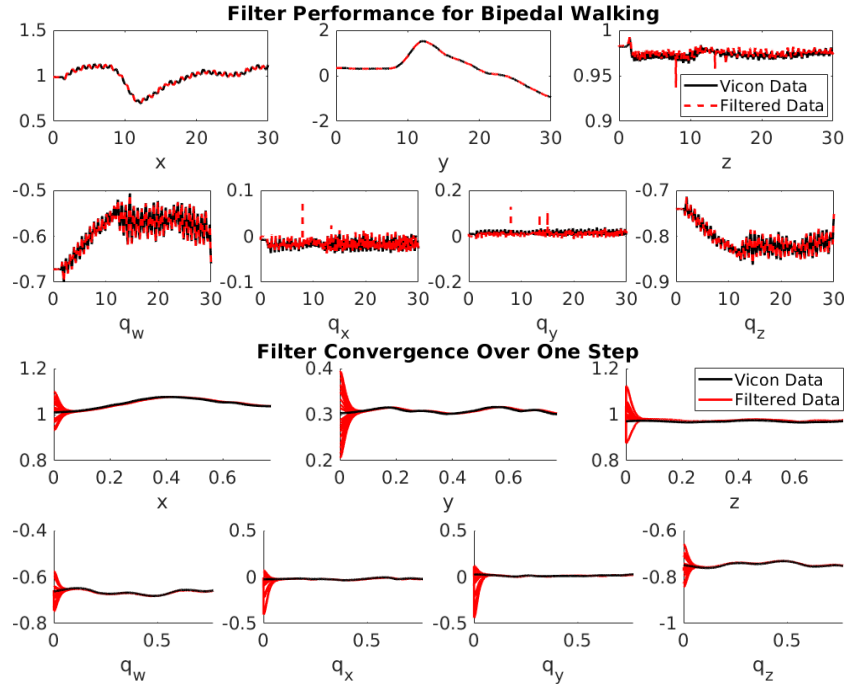
Fig. 5: The filter running on a Cassie series robot in a motion capture lab. Top: an example of a 30 second walking trajectory, we see good agreement between the motion capture data and the filtered estimate. Bottom: the filter performance during a typical step, starting from a 20 random initial estimates. Note that most of the initial estimates that underestimate the height are immediately corrected to the true height, preventing penetration with the floor. The one example that does not immediately track the correct height has a corresponding pitch/roll error that keep the feet above the ground.

we can see that the filter converges reliably to the true state within one step. The 30 second walking sequence demonstrates that the filter maintains good performance through many contact mode changes.

On a large robot like Cassie, the filter operates at an average of 174 Hz. Although the underlying optimization problem is an MIQP, the contact mode changes much more slowly than the filter update frequency, so we can achieve fast performance by warm starting the contact mode in the optimization problem. This allows the optimizer to quickly prune the branch-and-bound tree and arrive at the globally optimal solution in fewer iterations. Figure 6 illustrates the advantage of warm starting the optimization with the last contact mode.

Slipping Estimation while walking in ideal scenarios—e.g., where the probability of slipping is very small—is important, but it is also critical to maintain good state estimation during unplanned slipping events. To test the performance of the estimator in a highly dynamic contact scenario we lubricated one of the feet of our bipedal robot to encourage slipping. We executed a nominal walking controller that does not implement slip-recovery, causing the robot to fall on the
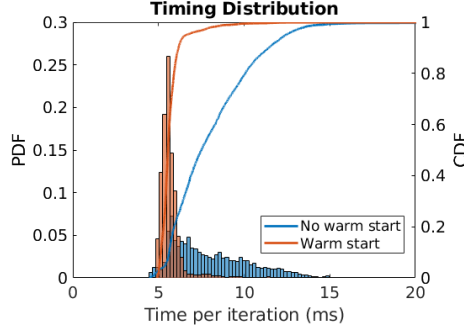
Fig. 6: The timing distribution for the filter running on Cassie walking data. Warm starting tightens the timing distribution and significantly decreases the mean update time.

first step. We compare the performance of the CCKF against the performance of a more traditional walking estimator based on the estimator developed for the Atlas robot during the DARPA Robotics Challenge [11].

For safety we conducted this test while the robot was attached to a harness outside of the motion capture lab. As a result we can only make qualitative comparisons between the filter results and a video of the experiment. However, these results clearly show that the walking estimator that relies on a no-slip assumption quickly accumulates large errors in floating base position, whereas the CCKF correctly predicts that the stance foot will slip while the floating base has minimal lateral motion. Repeating the slipping experiment while varying the orientation of the approximate friction polyhedron used by the filter produces virtually indistinguishable estimation results.

Parameter	Falling	Pushing	Bipedal Walking	Bipedal Slipping
P_0-position (m^2)	1×10^{-2}	1×10^{-5}	1×10^{-3}	1×10^{-3}
P_0-orientation	1×10^{-2}	1×10^{-3}	1×10^{-3}	1×10^{-3}
P_0-velocity $\left(\frac{m^2}{s^2}\right)$, $\left(\frac{rad}{s}\right)^2$	1×10^{-2}	1×10^{-2}	1×10^{-3}	1×10^{-3}
Q-position (m^2)	1×10^{-3}	1×10^{-6}	1×10^{-3}	1×10^{-3}
Q-orientation	1×10^{-3}	1×10^{-4}	1×10^{-3}	1×10^{-3}
Q-velocity $\left(\frac{m^2}{s^2}\right)$, $\left(\frac{rad^2}{s^2}\right)$	1×10^{-3}	1×10^{-4}	1×10^{-3}	1×10^{-3}
R-position (m^2)	1×10^{-3}	1×10^{-5}	1×10^{-2}	N/A
R-orientation	1×10^{-3}	1×10^{-3}	1×10^{-2}	1×10^{-2}
R-angular rate $\left(\frac{rad^2}{s^2}\right)$	1×10^{-3}	N/A	1×10^{-6}	1×10^{-6}
R-acceleration $\left(\frac{m^2}{s^4}\right)$	1×10^{-3}	N/A	N/A	N/A
R-joint data (rad^2), $\left(\frac{rad^2}{s}\right)$	N/A	N/A	1×10^{-6}	1×10^{-6}

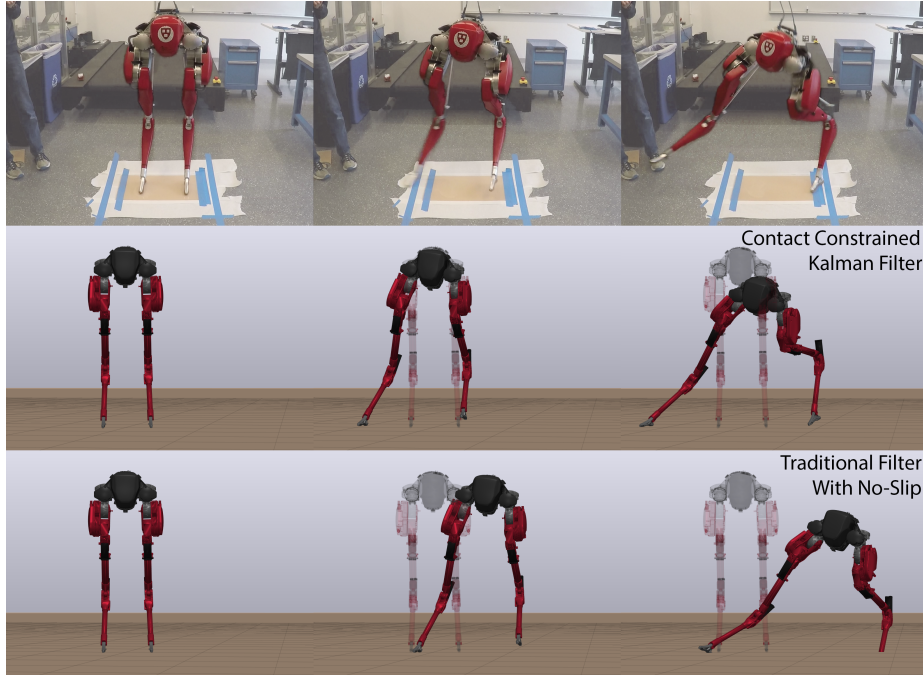Table 1: Filter covariance parameters used in the experiments presented here.

Fig. 7: Top: Video frames at key moments of the slip. Middle: The state estimated by the CCKF. Bottom: The state estimated by a filter that factors out the joints from the floating base and uses a no-slip assumption at the feet.

6   Conclusion

We developed a constrained Kalman filter as an approximate MAP estimator for rigid body systems with frictional contact and evaluated its performance in several simulated and physical estimation tasks. In addition to addressing some fundamental problems that arise from sample-based estimators, our results suggest that the filter performs well through sliding and collision events. We also demonstrated scalability of the algorithm, despite its non-convexity, by estimating the state of a 20-DoF bipedal robot in realtime.

Although the filter demonstrates good empirical performance, we provide no theoretical guarantees on the convergence. In fact, it is not difficult to generate examples in which the discontinuous contact events produce multimodal distributions that may cause the filter to diverge. In such a scenario it may be desirable to represent multimodal belief distributions or to estimate the distribution over contact modes in a similar fashion to the Contact Particle Filter [15]. In practice, it may be possible to solve the problem of multimodality by having sufficient measurement power. For example, even if a contact event causes the prior distribution to become multimodal, the right information from the sensors during the likelihood update can allow the filter to choose the correct mode.

It is also worth noting that although we show good empirical performance when solving the optimization problem described by (23) and (24), the number of contact modes grows exponentially with the number of contact pairs. This sug-

gests that for a larger number of contacts the problem may become intractable, and different solution methods for solving the QPCC should be considered.

Another limitation of the CCKF is that it assumes knowledge of the geometry and frictional properties of contact with the environment. Even in cases where local contact geometry can be accurately measured, it may be necessary to estimate the coefficient of friction online. In fact, recent work has demonstrated that even in controlled environments it may not be valid to assume that the coefficient of friction is constant, but rather that it should be treated as a random variable that follows some distribution [27]. An alternative approach would be to use a dual estimator to estimate the contact parameters, such as friction and geometry, simultaneously with the state. Recent work has shown that many popular contact models lack the descriptive ability to describe phenomena such as back-spin [28] and data-driven contact models can significantly outperform purely theoretical approaches [29].

7   Acknowledgements

References

1. G. Wahba, "A Least Squares Estimate of Satellite Attitude," *SIAM Rev.*, vol. 7, pp. 409–409, July 1965.
2. D. Simon, "Kalman filtering with state constraints: A survey of linear and nonlinear algorithms," *IET Control Theory Applications*, vol. 4, pp. 1303–1318, Aug. 2010.
3. D. E. Stewart and J. C. Trinkle, "An implicit time-stepping scheme for rigid body dynamics with inelastic collisions and coulomb friction," *International Journal for Numerical Methods in Engineering*, vol. 39, no. 15, pp. 2673–2691, 1996.
4. K. Lowrey, J. Dao, and E. Todorov, "Real-time State Estimation with Whole-Body Multi-Contact Dynamics: A Modified UKF Approach," in *Proceedings of the IEEE-RAS International Conference on Humanoid Robots*, 2016.
5. S. Kajita, F. Kanehiro, K. Kaneko, K. Fujiwara, K. Yokoi, and H. Hirukawa, "Biped walking pattern generation by a simple three-dimensional inverted pendulum model," *Advanced Robotics*, vol. 17, pp. 131–147, Jan. 2003.
6. B. J. Stephens, "State estimation for force-controlled humanoid balance using simple models in the presence of modeling error," in *2011 IEEE International Conference on Robotics and Automation*, pp. 3994–3999, May 2011.
7. S. Wang, Y. Shi, X. Wang, Z. Jiang, and B. Yu, "State estimation for quadrupedal using linear inverted pendulum model," in *2017 2nd International Conference on Advanced Robotics and Mechatronics (ICARM)*, pp. 13–18, Aug. 2017.
8. M. Bloesch, M. Hutter, M. A. Hoepflinger, S. Leutenegger, C. Gehring, C. D. Remy, and R. Siegwart, "State Estimation for Legged Robots - Consistent Fusion of Leg Kinematics and IMU," 2012.
9. N. Rotella, M. Bloesch, L. Righetti, and S. Schaal, "State estimation for a humanoid robot," in *2014 IEEE/RSJ International Conference on Intelligent Robots and Systems*, pp. 952–958, Sept. 2014.

10. X. Xinjilefu, S. Feng, and C. G. Atkeson, "Dynamic state estimation using Quadratic Programming," in *2014 IEEE/RSJ International Conference on Intelligent Robots and Systems*, pp. 989–994, Sept. 2014.

11. S. Kuindersma, R. Deits, M. Fallon, A. Valenzuela, H. Dai, F. Permenter, T. Koolen, P. Marion, and R. Tedrake, "Optimization-based locomotion planning, estimation, and control design for Atlas," *Autonomous Robots*, vol. 40, no. 3, pp. 429–455, 2016.

12. R. Hartley, J. Mangelson, L. Gan, M. G. Jadidi, J. M. Walls, R. M. Eustice, and J. W. Grizzle, "Legged Robot State-Estimation Through Combined Forward Kinematic and Preintegrated Contact Factors," *arXiv:1712.05873 [cs]*, Dec. 2017.

13. S. P. N. Singh and K. J. Waldron, "A Hybrid Motion Model for Aiding State Estimation in Dynamic Quadrupedal Locomotion," in *Proceedings 2007 IEEE International Conference on Robotics and Automation*, pp. 4337–4342, Apr. 2007.

14. F. Nori, N. Kuppuswamy, and S. Traversaro, "Simultaneous state and dynamics estimation in articulated structures," in *2015 IEEE/RSJ International Conference on Intelligent Robots and Systems (IROS)*, pp. 3380–3386, Sept. 2015.

15. M. C. Koval, N. S. Pollard, and S. S. Srinivasa, "Pose estimation for planar contact manipulation with manifold particle filters," *The International Journal of Robotics Research*, vol. 34, pp. 922–945, June 2015.

16. M. C. Koval, M. Klingensmith, S. S. Srinivasa, N. S. Pollard, and M. Kaess, "The manifold particle filter for state estimation on high-dimensional implicit manifolds," pp. 4673–4680, IEEE, May 2017.

17. K. Lowrey, S. Kolev, Y. Tassa, T. Erez, and E. Todorov, "Physically-consistent sensor fusion in contact-rich behaviors," in *2014 IEEE/RSJ International Conference on Intelligent Robots and Systems*, pp. 1656–1662, Sept. 2014.

18. D. Baraff, "Fast contact force computation for nonpenetrating rigid bodies," pp. 23–34, ACM Press, 1994.

19. C. E. Lemke and J. T. Howson and Jr., "Equilibrium Points of Bimatrix Games," *Journal of the Society for Industrial and Applied Mathematics*, vol. 12, no. 2.

20. M. C. Ferris and T. S. Munson, "Interfaces to PATH 3.0: Design, Implementation and Usage," *Computational Optimization and Applications*, vol. 12, pp. 207–227, Jan. 1999.

21. M. Anitescu and F. A. Potra, "Formulating dynamic multi-rigid-body contact problems with friction as solvable linear complementarity problems," *Nonlinear Dynamics*, vol. 14, no. 3, pp. 231–247, 1997.

22. "Bullet Collision Detection & Physics Library." http://www.bulletphysics.org/.

23. R. Smith, "Open Dynamics Engine." http://www.ode.org/, 2007.

24. "DART: Dynamic Animation and Robotics Toolkit." https://dartsim.github.io/.

25. Gurobi Optimization, Inc., "Gurobi Optimizer Reference Manual," tech. rep., 2014.

26. R. Tedrake and the Drake Development Team, "Drake: A planning, control, and analysis toolbox for nonlinear dynamical systems," 2016.

27. K.-T. Yu, M. Bauza, N. Fazeli, and A. Rodriguez, "More than a Million Ways to Be Pushed: A High-Fidelity Experimental Dataset of Planar Pushing," *arXiv:1604.04038 [cs]*, Apr. 2016.

28. N. Fazeli, S. Zapolsky, E. Drumwright, and A. Rodriguez, "Fundamental Limitations in Performance and Interpretability of Common Planar Rigid-Body Contact Models," *arXiv:1710.04979 [cs]*, Oct. 2017.

29. N. Fazeli, R. Kolbert, R. Tedrake, and A. Rodriguez, "Parameter and contact force estimation of planar rigid-bodies undergoing frictional contact , Parameter and contact force estimation of planar rigid-bodies undergoing frictional contact," *The International Journal of Robotics Research*, vol. 36, pp. 1437–1454, Dec. 2017.